

Journal of Biomedical Optics

SPIEDigitalLibrary.org/jbo

LipImage™ 815: novel dye-loaded lipid nanoparticles for long-term and sensitive *in vivo* near-infrared fluorescence imaging

Aurélie Jacquart
Michelle Kéramidas
Julien Vollaire
Raphaël Boisgard
Géraldine Pottier
Emilie Rustique
Frédérique Mittler
Fabrice P. Navarro
Jérôme Boutet
Jean-Luc Coll
Isabelle Texier

Liplmage™ 815: novel dye-loaded lipid nanoparticles for long-term and sensitive *in vivo* near-infrared fluorescence imaging

Aurélie Jacquart,^a Michelle Kéramidas,^b Julien Vollaire,^b Raphaël Boisgard,^c Géraldine Pottier,^c Emilie Rustique,^a Frédérique Mittler,^a Fabrice P. Navarro,^a Jérôme Boutet,^a Jean-Luc Coll,^b and Isabelle Texier^a

^aCEA Grenoble, LETI-DTBS, MINATEC campus, F38054 Grenoble, France

^bINSERM-UJF U823, Institut Albert Bonniot, 38706 Grenoble, France

^cSHFJ, CEA Orsay, 4 place Général Leclerc, 91401 Orsay Cedex, France

Abstract. A new contrast agent, Liplmage™ 815, has been designed and compared to previously described indocyanine green (ICG)-loaded lipid nanoparticles (ICG-lipidots®). Both contrast agents display similar size (50-nm diameter), zeta potential, high IC50 in cellular studies, near-infrared absorption and emission wavelengths in the “imaging window,” long-term shelf colloidal and optical stabilities with high brightness ($>10^6$ L mol⁻¹ cm⁻¹) in ready-to-use storage conditions in aqueous buffer (4°C in dark), therefore being promising fluorescence contrast agents for *in vivo* imaging. However, while ICG-lipidots® display a relatively short plasma lifetime, Liplmage™ 815 circulates in blood for longer times, allowing the efficient uptake of fluorescence signal in human prostate cancer cells implanted in mice. Prolonged tumor labeling is observed for more than 21 days. © 2013 Society of Photo-Optical Instrumentation Engineers (SPIE) [DOI: 10.1117/1.JBO.18.10.101311]

Keywords: fluorescence imaging; lipid nanoparticles; organic dyes; ICG.

Paper 130109SSR received Feb. 28, 2013; revised manuscript received Jun. 7, 2013; accepted for publication Jun. 27, 2013; published online Jul. 30, 2013.

1 Introduction

In the last 10 years, *in vivo* near-infrared (NIR) fluorescence imaging has emerged from preclinical studies to the medical field.^{1–3} With its high sensitivity, ease of manipulation, and reduced cost in comparison to other molecular imaging techniques such as magnetic resonance imaging, positron emission tomography, or single-photon emission computed tomography, fluorescence imaging is now opening the way to new medical practices in diagnostics^{4,5} and surgery.^{6–12}

Instrumental developments are nowadays mature; however, clinical *in vivo* fluorescence imaging still suffers from the short list of human-use approved fluorophores, namely, indocyanine green (ICG, LD50 of 50 to 80 mg/kg for animal subjects¹³) and methylene blue (LD50 of 1180 mg/mL in rats).^{14,15} The limitations associated with the use of these dyes when injected as such (i.e., in their free form in aqueous buffers), have already been underlined: poor optical properties,^{15–19} aggregation issues, and strong adsorption on plasma proteins,^{16,17} which ultimately govern their biodistribution.²⁰ Different nanoparticle templates were proposed to improve the vectorization of these dyes^{21–30} with limited success, mainly because of poor dye payload without selfquenching²⁷ or poor encapsulation stability²⁸ with time or upon injection.^{22,24,29,30} We previously described ICG-loaded lipid nanoparticles (ICG-Lipidots®) as very bright objects, with outstanding dye-encapsulation stability in storage conditions (>1 year with fluorescence quantum yield >0.08 in 1X phosphate buffer saline (PBS), <17% dye leakage in 40 days).^{31,32} These nanocontrast

agents were successfully used to label lymph nodes (intradermal injection) or Ts-/Apc-xenografted tumors in nude mice (intravenous injection).³¹ Fluorescence signal was observed in the tumor and the liver with higher intensity than that recorded after the injection of the free dye. ICG-Lipidots® allowed prolonged tumor detection up to 48 h and displayed 1.9 times higher tumor/skin ratio (from 24 to 48 h) than free ICG formulated in glycosylated water. However, the overall fluorescence signal dropped dramatically 5 h after injection. This could be accounted for by the fact that ICG, as an amphiphilic dye (log *P* = 2.1), is included in the nanoparticle shell rather than entrapped in the lipid particle core, as was demonstrated by nuclear magnetic resonance (NMR).³³ ICG leakage from the nanoparticle shell after their injection could also be favored by particle interactions with plasma proteins, for which ICG affinity is very strong.^{16,17} On the contrary, highly lipophilic dyes (for instance, DiD with log *P* > 10), for which C18 alkyl chains are included in their structure, demonstrated efficient core anchoring in the lipid nanoparticles (NMR evidence),³³ associated with prolonged labeling of lymph nodes.³⁴ However, their absorption and emission wavelengths are not optimized for sensitive in-depth tissue imaging.

These previous results inspired us to design a new NIR fluorophore with optical properties in the most suitable wavelength range for *in vivo* imaging (≈ 800 nm),^{35,36} and optimized structural properties for its efficient and prolonged encapsulation in the core of lipid nanoparticles. These nanoparticles are very interesting nanovectors with respect to *in vivo* applications for several purposes: they are based on human-use approved ingredients with high biocompatibility and their fabrication process is free of toxic solvents and has already been scaled up for cosmetic applications.^{37,38} The commercial IR780 dye

Address all correspondence to: Isabelle Texier, CEA Grenoble, LETI-DTBS, MINATEC campus, F38054 Grenoble, France. Tel: +33 438 784 670; Fax: +33 438 785 787; E-mail: isabelle.texier-nogues@cea.fr, or Jean-Luc Coll, INSERM-UJF U823, Institut Albert Bonniot, 38706 Grenoble, France. Tel: +33 4 76 54 95 53; Fax: +33 4 76 54 94 13; E-mail: Jean-Luc.Coll@ujf-grenoble.fr

was therefore modified with one C18 alkyl chain to yield a highly lipophilic IR780-lipid fluorophore ($\log P > 10$) which, encapsulated in lipid nanoparticles, lead to a new nanoimaging agent named LipImage™ 815. The present study focusses on the optical properties of this new contrast agent in comparison to previously described ICG-Lipidots®. With a higher fluorescence quantum yield in the same wavelength range, similar to very low cytotoxicity, LipImage™ 815 displays a prolonged plasma circulation in mice as well as a never reported long-term imaging of tumors (>2 weeks).

2 Materials and Methods

2.1 Materials

Suppocire NB™ was purchased from Gattefossé (Saint-Priest, France), Lipoid S75 (soybean lecithin at >75% phosphatidylcholine) from Lipoid (Ludwigshafen, Germany), Myrj™ S40 (polyethylene glycol 40 stearate), and super refined soybean oil from Croda Uniqema (Chocques, France). ICG, IR780 iodide dye, and other chemicals were purchased from Sigma-Aldrich (Saint-Quentin-Fallavier, France).

2.2 LipImage™ 815 Preparation

The IR780-lipid dye was synthesized in two steps using commercial IR780 iodide as a starting material. In the first step, a carboxylic acid group was introduced in the fluorophore template using the same procedure as previously described for the IR786 dye.³⁹ A C₁₈ lipid chain was then grafted on the fluorophore using oleylamine and standard $-\text{CO}_2\text{H}/\text{NH}_2$ coupling chemistry activated by benzotriazol-1-yloxytris(dimethylamino)phosphonium hexafluorophosphate (BOP).

An oil premix with, respectively, 85, 255, and 65 mg of oil, Suppocire NB™ and lecithin was prepared. IR780-lipid dye solution (200 μL) in ethanol (10 mg/mL) was poured in a 5-mL vial and mixed with the oil premix melted at 50°C. The mixture was homogenized and the solvent was then evaporated under argon flux. After homogenization at 50°C, the continuous aqueous phase, composed of 345 mg of Myrj™ S40 and the appropriate amount of aqueous solution (154 mM NaCl if not stated otherwise, qsp 2 mL), was introduced. The vial was placed in a 50°C water bath and the mixture was sonicated for 5 min using a VCX750 Ultrasonic processor (power output 190 W, 3-mm probe diameter, Sonics). LipImage™ 815 was dialyzed overnight at room temperature against 1000 times their volume in the appropriate aqueous buffer (12 to 14,000 Da MW cut off membranes, ZelluTrans, Carl Roth, France). Finally, the nanoparticle dispersion was filtered through a 0.22 μm Millipore membrane for sterilization before characterization and/or injection.

2.3 Size and Zeta Potential Measurements

Dynamic light scattering (DLS) was used to determine the particle hydrodynamic diameter and zeta potential (Zeta Sizer Nano ZS, Malvern Instrument, Orsay, France). Particle dispersions were diluted to 2 mg/mL of lipids in sterile 0.1X PBS and transferred in Zeta Sizer Nano cells (Malvern Instrument) before each measurement, performed in triplicate.

2.4 Dye Encapsulation Efficiency and Payload

The encapsulation efficiency of IR780-lipid dye in LipImage™ 815 was determined by spectrophotometric titration and

calculated by dividing the absorbance measured at 790 nm for freshly purified particle dispersion by the absorbance at 790 nm of the same particle dispersion before purification, by keeping the lipid concentration constant. The amount of dye which had been removed by dialysis was estimated. Absorbance was measured in 1X PBS using a UV-visible spectrophotometer (Cary 300 Scan, Varian, Les Ulis, France). The dye payload into the particles was obtained by calculation considering the initial dye amount in milligrams and the encapsulation efficiency.

2.5 Optical Properties

The absorbance and fluorescence measurements were performed in 1X PBS, respectively, using a Cary 300 Scan UV-visible spectrophotometer (Varian) and a Perkin Elmer LS50B fluorimeter. No scattering contribution was considered due to nanoparticle size and spectrum range (750 to 850 nm). Fluorescence quantum yields were calculated using ICG in dimethylsulfoxide (DMSO) ($\Phi = 0.13$) as a reference.⁴⁰

2.6 WST-1 In Vitro Cytotoxicity Assay

In accordance with the International Organization for Standardization (ISO) 10993, NIH-3T3 murine fibroblast cells were chosen to perform classical WST-1 cytotoxic assay (11644807001, Roche, Boulogne-Billancourt, France). The cell line was purchased from the American Type Culture Collection (3T3, CRL 1658, ATCC, Manassas, VA). Experimental cultures were prepared from deep-frozen stock vials and maintained in a subconfluent state in culture Petri Dish (113 cm²) under a humidified (90%) atmosphere of 95% air/5% CO₂ at 37°C. Cells were grown in Dulbecco's modified Eagle's medium high glucose (DMEM, 41966-029, Gibco, Invitrogen, Saint-Aubin, France) supplemented with 10% newborn calf serum (P30-0401, PAN Biotech GmbH, Aidenbach, Germany), and 1% antibiotics (penicillin and streptomycin) (15140-122, Gibco). Culture medium was changed every other day.

Cells (10⁴ cells/mL) were seeded in 96-well plates (Nunc, Sigma-Aldrich, Saint-Quentin-Fallavier, France). After 24-h incubation at 37°C, different concentrations of lipid nanoparticles, from 50 to 1500 $\mu\text{g}/\text{mL}$ (7.2×10^{11} to 2.2×10^{13} particles/mL), were added for 24 h to the culture medium. Each group had sixplicate wells. Cytotoxicity was assessed 24 h following the nanoparticle removal using WST-1 assay, analogue to MTT assay. WST-1 reagent (Roche, Boulogne-Billancourt, France) was added (10%) to the culture medium and kept in the incubator for 3 h. Cells without nanoparticles and those incubated with a solution of H₂O₂ 10 mM were, respectively, used as negative and positive controls. Absorbance was then recorded at 450 nm (soluble formazan titration) and 690 nm (background subtraction) using a microplate reader (Infinite M1000, Tecan, Lyon, France). The absorbance difference (450 to 690 nm) was directly proportional to the number of viable cells. Cell viability was expressed as a percentage of viable cells as determined using the following equation: $\text{Viability}(\%) = [(A_S - A_{PC}) / (A_{NC} - A_{PC})] \times 100$; where A_S , A_{PC} , and A_{NC} represented absorbances of the sample, the positive control (cells with H₂O₂ 10 mM), and the negative control (only cells), respectively. Data were compared among groups by one-way ANOVA followed by Fisher's protected least significance differences test.

2.7 In Vivo Imaging Experiments

All animal procedures were in compliance with the guidelines of the European Union (regulation N°86/609), taken in the French law (decree 87/848) regulating animal experimentation. All efforts were made to minimize animal suffering and to reduce the number of animals used. All animal manipulations were performed with sterile techniques and were approved by the Rhône-Alpes Animal Care and Use committee (France) or by the animal ethics committee of Institut d'Imagerie Biomédicale.

To assess the biodistribution of Liplmage™ 815 in comparison to free IR780-lipid dye dispersed in 5% ethanol/95%NaCl 154 mM, healthy FVB female mice (6 weeks old, Janvier, France), weighing 22 to 25 g, were injected through the tail vein in bolus with 100 μL volumes using 29G syringes. The injected doses corresponded to 8 nmol of dye and 1.3×10^{14} particles for Liplmage™ 815 (1.3×10^{15} particles/mL). Mice were anesthetized and sacrificed at different time points (30 min, 4 h, 24 h, $n = 3/\text{point}$), organs were harvested and their fluorescence analyzed using a Fluobeam®800 imaging set-up (Fluoptics, Grenoble, France). Fluobeam®800 is a compact and portable open-field NIR imaging system, combining fluorescence excitation by a 785-nm laser source and an optical head with a highly sensitive charge-coupled device (CCD) camera and white light-emitting diodes (LEDs) for field illumination. Dedicated optics scatter the laser and LEDs, enlightening a field of 6 cm in diameter at a distance of 17 cm. The power density of laser irradiation on tissue is $96 \mu\text{W}/\text{mm}^2$. The fluorescence signal is collected through a high-pass filter over 800 nm. Quantification of organ fluorescence was performed using the ImageJ® software, after subtraction of autofluorescence measured for each organ in control mice.

For histology and long-term biodistribution studies, 10 immunocompetent 6-week old BALB/cJ RJ mice were used. Nanoparticles (200 μL of solution containing 2×10^{15} nanoparticles/mL loaded with 300 μM of fluorophore, i.e., representing a dose of 60 nmol of dye, 4.0×10^{14} particles) were injected in the tail vein and animals were sacrificed at the indicated time points. The organs were then imaged with the fluoSTIC system for fluorescence detection. fluoSTIC is a previously described two-dimensional (2-D)-FRI system.⁴¹ Excitation was performed using a sub miniature A (SMA) coupled 500 mW, 740-nm laser diode from Power Technology (model# IQ1A) as NIR light source, and a SMA coupled 7-mW cold (5600K) white LED from Thorlabs

(model# MCWHF1). This system provides continuous NIR excitation of the body of the mouse because it produces a homogeneous lightened field (5 cm in diameter) with an illumination power of $10 \text{ mW}/\text{cm}^2$. The fluorescence signal is collected by a CM-030GE-RH (Jai, Denmark), 17-mm diameter camera with a 1/3 in monochrome CCD sensor and a resolution of 656×494 pixels. The filtration scheme of fluoSTIC accommodates an excitation filter centered at 740 nm that excites ICG with a 40% efficiency as well as an emission filter from 772 to 857 nm that collects most ICG emitted photons. All filters are interference filters purchased from Chroma (Bellows Falls, VT). A calibration curve was prepared from serial dilutions of particles (data not shown). Intensities of fluorescence were indicated as reference light units (RLU)/pixels/ms.

For plasmatic distribution, 6-week old BALB/cJ RJ mice received the same dose of nanoparticles in the tail vein (60 nmol of fluorophores, 4.0×10^{14} particles), and blood samples were collected at the indicated times from the tail vein. The blood was then centrifuged at 4°C at 2000 rpm, and the plasma was used to detect the presence of fluorescence. A drop of 20 μL was exposed to the fluoSTIC system and the amount of fluorescence was quantified as RLU/pixel/ms.

In the tumor model study, male athymic Swiss nude mice (Janvier, Le Genest-Isle, France) were used and maintained under specific pathogen-free conditions. A total of 10^7 human prostate cancer cells (PC3) in 200 μL phosphate-buffered saline were injected subcutaneously. When tumor diameter ranged between 5 and 8 mm (4 to 5 weeks), animals were injected intravenously with 200 μL of solution containing 2×10^{15} nanoparticles/mL loaded with 300 μM of fluorophore (60 nmol).

3 Results

3.1 Optical Properties of Liplmage™ 815

The commercial IR780 fluorophore, similarly to the IR-820 dye, is a heptacyanine dye presenting in its polymethine backbone a C6 ring for structure rigidification and improvement of optical and stability properties, as well as a chlorine group, which can be substituted by SN_1 substitution reactions as extensively described in the literature.^{39,42} Presenting suitable NIR optical properties for *in vivo* imaging (798-nm absorption, 819-nm emission in DMSO, Table 1), we reinforced its lipophilic

Table 1 Optical properties of Liplmage™ 815 and ICG-Lipidots® in PBS 1X ($n = 120$ dyes/particle), in comparison to free dyes in DMSO and ICG in glycosylated water. $\lambda_{\text{max}}(\text{abs})$, $\lambda_{\text{max}}(\text{em})$ are, respectively, the dyes absorption and emission maxima, ϵ is the molar extinction coefficient at the absorption maximum (/dye), Φ the fluorescence quantum yield, b the brightness. Brightness is defined as $b = \epsilon \times \Phi$ for free dyes, $b = n \times \epsilon \times \Phi$ for nanoparticles ($n = 120$ dyes/particle).

	$\lambda_{\text{max}}(\text{abs})$ (nm)	$\epsilon(\lambda_{\text{max}})$ ($\text{L mol}^{-1} \text{cm}^{-1}$)	$\lambda_{\text{max}}(\text{em})$ (nm)	Φ	Brightness ($\times 10^5 \text{ L mol}^{-1} \text{cm}^{-1}$)
Indocyanine green (ICG), glycosylated water	777	$150,000 \pm 5000$	803	0.048 ± 0.01	0.07 ± 0.01
ICG, DMSO	795	$215,000 \pm 5000$	821	0.13 ± 0.01	0.28 ± 0.01
IR780-lipid, DMSO	798	$150,000 \pm 5000$	819	0.12 ± 0.01	0.18 ± 0.01
ICG-Lipidots®	800	$200,000 \pm 5000$	820	0.06 ± 0.01	13 ± 1
Liplmage™ 815	793	$150,000 \pm 5000$	815	0.08 ± 0.01	12 ± 2

character by substituting the chlorine group with an oleyl chain to favor its anchoring in the lipid core of the particles.

ICG-Lipidots® and LipImage™ 815 lipid nanoparticles encapsulating, respectively, ICG and the newly designed IR780 lipid dye, were formulated following standard previously described procedures,^{34,37,38,43,44} leading to transparent green nanoparticle dispersions in aqueous buffer. DLS was used to assess ICG-Lipidots® and LipImage™ 815 hydrodynamic diameter, polydispersity, and zeta potential as well as the stability of the particle dispersions with time. The mean hydrodynamic diameter was 50 nm (polydispersity = 0.13) for both formulations and was not affected by dye payload. Nanoparticles were stable for more than 6 months while the formulations were stored at 4°C (Fig. 1). The same behavior was observed for zeta potential, which was -2.5 ± 0.5 mV for both the nanovectors. This neutral charge in NaCl or PBS buffer was accounted for by the dense PEG coating of the particle surface, which also ensured a high colloidal stability for the particles.

The dye encapsulation efficiency was assessed by spectrophotometric titration at the maximum of absorption comparing the optical absorption of freshly prepared solutions before and after dialysis. The difference allowed determining the amount of dye still encapsulated in the particle core. The entrapment efficiency of ICG-Lipidots® varied with the loading ratio (40% for low loading [ICG] < 10 dye/particle, 80% for higher loading $10 < [ICG] < 50$ dye/particle and decreased for very high loading > 50 dye/particle) for 30 nm nanoparticles.³¹ The entrapment efficiency of the IR780-lipid fluorophore in the nanoparticles remained above 70% for dye loading up to 330 dyes/particle (Fig. 2).

The optical features of LipImage™ 815 and ICG-Lipidots® (50-nm diameter particles loaded with 120 dyes/particle) dispersed in 1X PBS buffer in comparison to those of the non-encapsulated dyes in DMSO, and presently clinically used ICG in glycosylated water are presented in Table 1. The normalized absorbance and emission spectra of the particles are represented in Fig. 3. IR780-lipid dye displayed similar optical properties to ICG in DMSO, with absorbance maximum at 798 versus 795 nm for ICG, emission maximum at 819 versus 821 nm for ICG, fluorescence quantum yield of 0.12 versus 0.13 for ICG. Freshly prepared ICG in glycosylated water presented blue-shifted absorption and emission as well as reduced

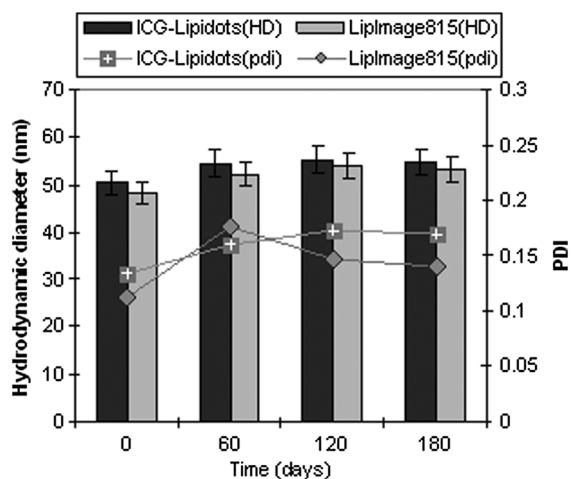


Fig. 1 Evolution of the hydrodynamic diameter and polydispersity (PDI) of the nanoparticle dispersions during storage at 4°C in the dark.

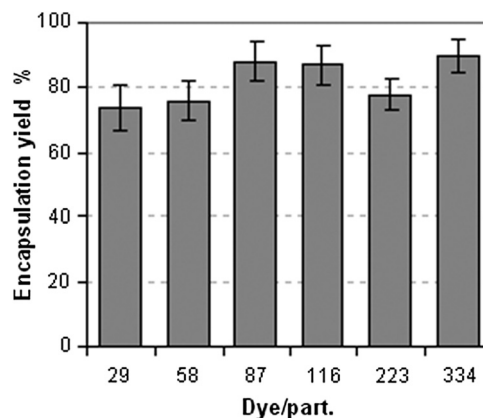


Fig. 2 Influence of dye loading on encapsulation efficiency for LipImage™ 815.

fluorescence quantum yield (0.048).³¹ Molar extinction coefficient was lower for IR780-lipid dye than that of ICG, $150,000 \text{ L mol}^{-1} \text{ cm}^{-1}$ versus $215,000 \text{ L mol}^{-1} \text{ cm}^{-1}$, leading to brightness for the free dye in DMSO 1.5-fold lower than for ICG. LipImage™ 815 and ICG-Lipidots® showed optical properties close to those of the free dyes in DMSO: the absorbance and emission maxima were slightly blue shifted (5 nm) for IR780-lipid dye, showing a low positive solvatochromism from the apolar oily core of the nanoparticle to highly polar DMSO. This effect was not observed for free and encapsulated ICG where the absorbance maximum was slightly red shifted. For both the dyes, molar extinction coefficients were not influenced or were slightly influenced by encapsulation. Fluorescence quantum yields slightly decreased upon encapsulation, from 0.13 to 0.06 for ICG-Lipidots® and from 0.12 to 0.08 for LipImage™ 815 (Table 1). However, fluorescence quantum yields of the LipImage™ 815 and ICG-Lipidots® dispersions remained unchanged over 3 months during storage at 4°C in the dark in aqueous buffer (Fig. 4), whereas glycosylated ICG, with lower fluorescence quantum yield, aggregated and became nonfluorescent in a few hours.¹⁹ The IR780-lipid dye was not soluble at all in aqueous buffer. The fluorescence quantum yield of LipImage™ 815 was stable for dye payloads up to 330 dyes/particle at least, allowing the achievement of highly bright nanoparticles (Fig. 5). The stability of the fluorescence

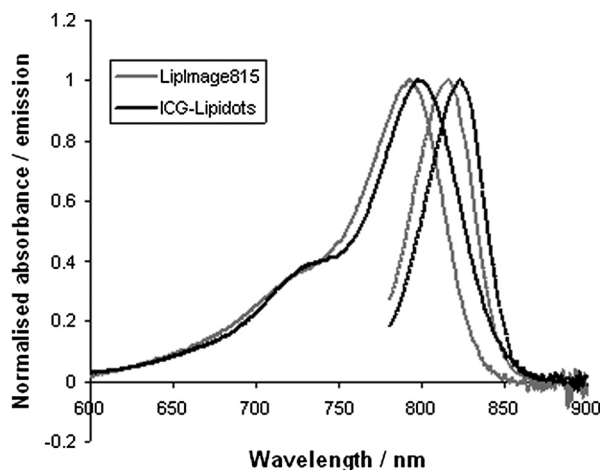


Fig. 3 Normalized absorption and emission spectra of LipImage™ 815 and ICG-Lipidots® in 1X PBS (excitation at 750 nm).

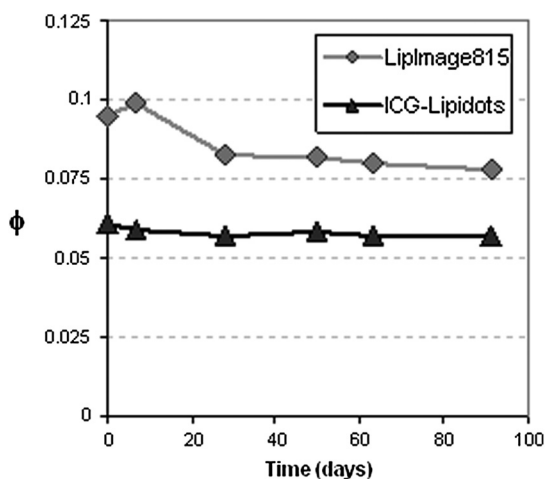


Fig. 4 Time evolution at 4°C in darkness of the fluorescence quantum yields of LipImage™ 815 and ICG- Lipidots® in 1X PBS (excitation at 750 nm).

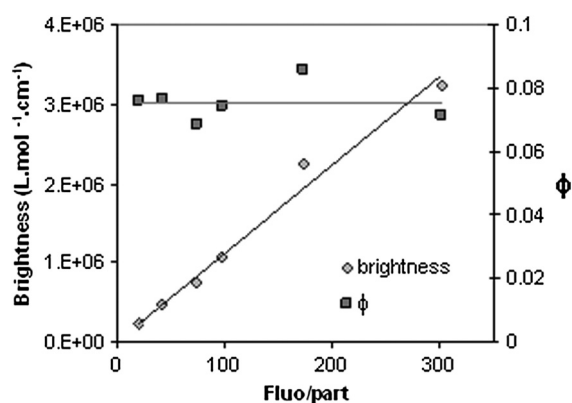


Fig. 5 Influence of dye loading on fluorescence quantum yield and particle brightness for LipImage™ 815.

quantum yield over the increasing dye loading evidenced an absence of self-quenching and aggregation of the dye in the lipid core. Overall, LipImage™ 815 and ICG-Lipidots® displayed similar optical properties in terms of absorption and emission wavelengths and brightness. Encapsulation of the dyes in the lipid formulation ensured their prolonged preservation of both colloidal and optical properties, while stored in ready-to-use conditions (solvent-free saline buffer).

3.2 *In Vitro* Cytotoxicity

The cytotoxicity of different nanoparticle dispersions, naked Lipidots®, ICG-Lipidots® and the novel NIR probe LipImage™ 815, was assessed on NIH 3T3 fibroblasts through a cell viability assay (WST-1) (Fig. 6). The toxicity profiles of these nanoformulations were relatively similar, all of them exhibiting a half-maximal inhibitory concentration close to the high lipid concentration of 1 mg/mL, corresponding to 1.5×10^{13} particles/mL. This indicated that (1) lipid nanoparticles were very well tolerated by fibroblasts in culture for an incubation time of 24 h and (2) the incorporation of a NIR dye for *in vivo* imaging purpose (either ICG or IR780-lipid dye) did not modify the toxicity index of the basic formulation.

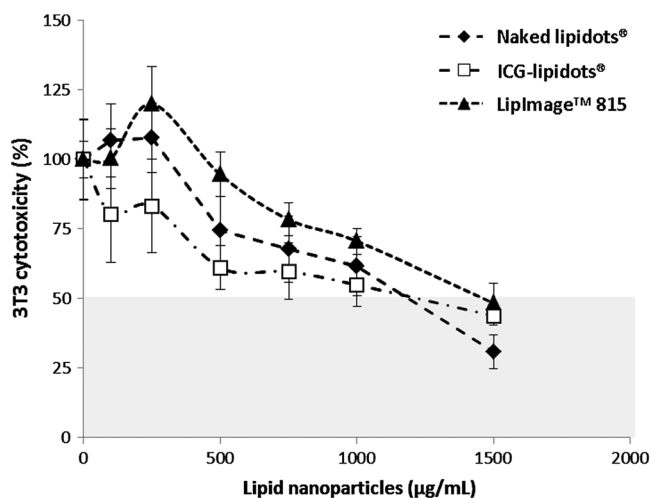


Fig. 6 Cell viability assay (WST-1) on NIH 3T3 fibroblasts after 24-h incubation of different particle dispersions: naked Lipidots® (black diamond), ICG-Lipidots® (white square), and LipImage™ 815 (black triangle).

3.3 *In Vivo* Imaging

First, the biodistribution of LipImage™ 815 and of the free IR780-lipid dye was assessed in FVB healthy mice (Fig. 7). Fluorescence was relatively homogeneously distributed through the different organs after LipImage™ 815 injection, even if more pronounced in liver, and to a lesser extent in steroid-rich organs (adrenals, ovaries). On the contrary, injection of the IR780-lipid dye dispersed in water/ethanol mixture led to massive fluorescence signal in spleen and liver in a few hours after injection.

The absence of toxicity consecutive to a systemic administration of LipImage™ 815 was further checked in long-term experiments. For this purpose, 10 mice receive 200 μL of the LipImage™ 815 formulation (60 nmol of fluorophores, 4.0×10^{14} particles), and two of them were sacrificed at 24 h after injection, two others at 8 days and two others at 15 days. The remaining four mice were followed till day 21. No signs of toxicity were noticed, i.e., no weight loss, no obvious reaction was visible on the live mice. In addition, after a histologic examination using HES coloration (hematoxylin, eosin, safran) of frozen sections of liver, spleen, lungs, or kidneys, all tissues appeared normal (data not shown). At days 1, 8, 15, and 21, the main organs were also exposed to the NIR camera in order to detect the presence of fluorescence. Biodistribution was similar to that reported in Fig. 7, with a global decrease of fluorescence in all organs starting at day 1 (except liver for which a slight increase was observed between day 1 and day 8). However, the fluorescence signal associated with the LipImage™ 815 injection was still very elevated at day 8, until day 21.

Another series of mice was used for the evaluation of the blood clearance of ICG-Lipidots® and LipImage™ 815. Three mice received LipImage™ 815 intravenously, and three others the same dosage of ICG-Lipidots®. Blood samples were collected at 15 min, 30 min, 1 h, 3 h, and 5 h after systemic administration of ICG-Lipidots®, while we also collected a sample of blood at 24 h for LipImage™ 815. As can be seen in Fig. 8, the fluorescence signal present in the plasma was very low and disappeared extremely rapidly when ICG-

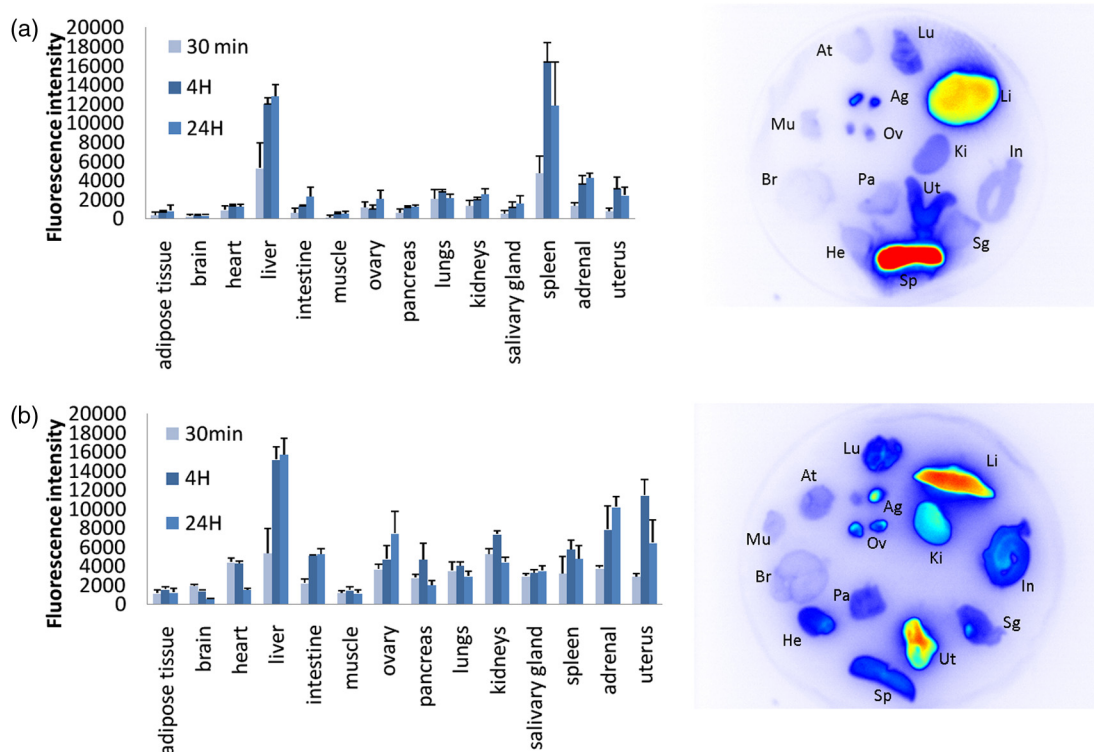


Fig. 7 Fluorescence biodistribution 24 h after injection of IR780-lipid dye (a) or LipImage™ 815 (b) in FVB mice. At, adipose tissue; Ag, adrenal glands; Br, brain; He, heart; In, intestines; Ki, kidney; Li, liver; Lu, lung; Mu, muscle; Ov, ovaries; Pa, pancreas; Sg, salivary gland; Sp, spleen; Ut, uterus.

Lipidots® were injected (0.6% of the injected dose at 30-min postinjection), while 7.5% of the injected dose was present at 30-min postinjection for LipImage™ 815, 2.5% at 5 h and still 0.5% one day later. This indicated that LipImage™ 815 remained in circulation in the blood stream for extended periods of time before being completely eliminated.

This long lasting circulation was associated with a very good tumor enhanced permeability and retention (EPR) effect, as can be seen in Fig. 9(a). In two nude mice bearing PC3 subcutaneous prostate tumors, fluorescence was detected noninvasively at the tumor site till 22 days after injection of LipImage™ 815. At

this time, the signal was still very elevated and easily detectable using 20 ms exposure time, as shown for mouse #1 (mouse #2 was similar). We then reproduced this experiment in three other mice with the same prostate tumors. As presented in Figs. 9(b) and 9(c), the passive, EPR-guided, accumulation of LipImage™ 815 in the tumors provided tumor/skin ratio ranging between 2 and 3.4. The best signal/noise ratio was obtained at day 9, demonstrating again the long-term persistence of the signal in the tumors although the intensity of the signal was gradually declining over time.

4 Discussion

ICG-Lipidots® and LipImage™ 815 are both nanocontrast agents based on dye-loaded lipid nanoparticles. The particle lipid core is composed of a mixture of soybean oil and a wax, which results in an oily mixture of C₈ to C₁₈ mono-, di- and tri-glycerides, solid at ambient temperature and liquid around 35°C.^{31,32,34,44} The surfactant shell is composed of a mixture of lecithin (phospholipids) and stearate-PEG surfactants bearing long poly(ethyleneglycol) (PEG) chains. The main drawback of nanoemulsions—namely intrinsic poor colloidal stability—has been overcome by the use of a complex mixture of core lipids and surfactants: mixing entropy stabilizes the physicochemical system.³⁸ The manufacturing process is free of toxic solvents, highly robust, easy to implement on an industrial scale, and based on low cost biocompatible and human-use approved ingredients.

The physicochemical properties of LipImage™ 815 are similar to those of ICG-Lipidots® concerning hydrodynamic diameter, zeta potential, and long-term colloidal stability of the particle dispersions on the shelf. Loading of the IR780-lipid dye in the particle is highly efficient (>70% yield, up to 330 dyes/particle) thanks to the presence of a C18 lipophilic

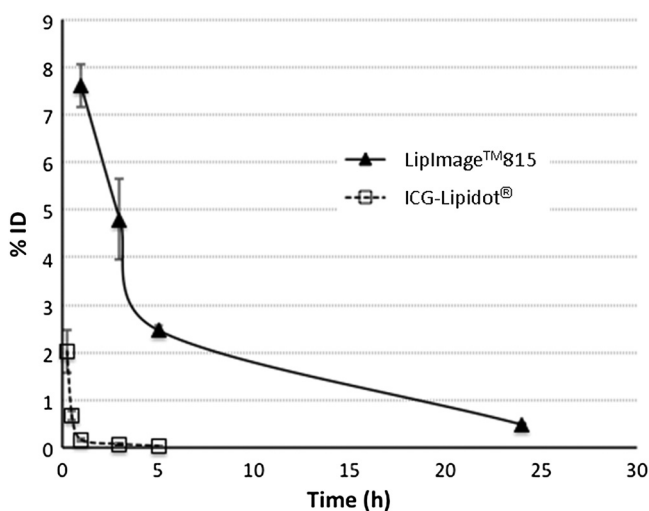


Fig. 8 Fluorescence in plasma after injection of ICG-lipidots® or LipImage™ 815 in BALB/cJ mice.

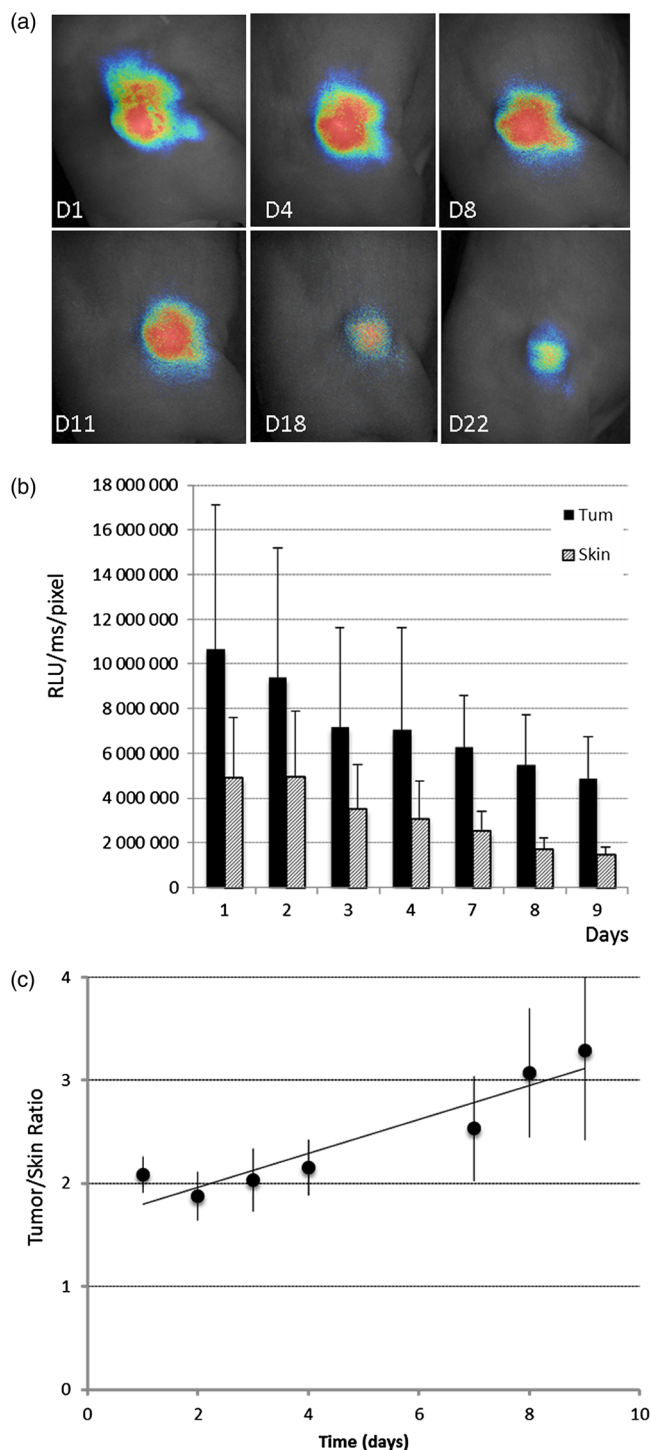


Fig. 9 Fluorescence accumulation in tumor after LipImage™ 815 injection in athymic Swiss nude mice with implanted human prostate cancer cells (PC3). (a) *In vivo* fluorescence images of the tumor at days 1, 4, 8, 11, 18, 22 and (b) quantification of the fluorescence signal in tumor and skin. (c) Tumor over skin fluorescence ratio.

chain in its structure, which should ensure the anchoring of the fluorophore in the nanoparticle core as observed previously for other C18 dyes such as DiO, DiI, or DiD³⁴ rather than in the particle shell as observed for ICG.³³ The stability of the fluorescence quantum yield while increasing dye payload also evidences the absence of fluorescence self-quenching and dye aggregation in the explored range of fluorophore loading.

These two results (high dye encapsulation efficiency and absence of self-quenching in the particle) demonstrate the good solubility of the IR780-lipid dye in the oily core of the particles in the explored concentration range (up to 1.6 mM of dye locally in the particle core). In conclusion, LipImage™ 815 and ICG-Lipidots® display similar optical properties in terms of absorption and emission wavelengths, brightness, ease of production, and shelf stability, which make them both attractive objects for *in vivo* fluorescence imaging contrast agents. However, significant differences are observed during *in vivo* experiments.

In vivo experiments were performed at doses of 1.3×10^{14} to 4.0×10^{14} particles. Considering that the total blood volume of mice (25 g) is around 1.8 mL (7.25% of mouse weight), the concentration of particles in blood just after injection was $\approx 0.7 \times 10^{14}$ to 2.0×10^{14} particles/mL. This concentration was 10-fold the one used in the cytotoxicity experiments performed on NIH 3T3 fibroblasts, for which a IC_{50} level superior to 1 mg/mL of lipids (1.5×10^{13} particles/mL) was observed. Considering blood cell concentration around 10^9 cells/mL, particles per cell ratios were 1.5×10^9 and 0.7×10^5 to 2.0×10^5 , respectively, for the *in vitro* assays and *in vivo* experiments. Therefore, *in vivo* experiments were performed at doses far under the IC_{50} cell level as far as comparisons can be made.

As previously reported for other lipophilic dyes such as DiD,⁴⁵ the fate of the IR780-lipid fluorophore is completely modified by its encapsulation in the core of the lipid particles. The important spleen uptake observed for the free dye is reduced, and a more homogeneous distribution in mice body is achieved as well as a prolonged circulation in plasma. The biodistribution and pharmacokinetics of LipImage™ 815 are in agreement with the biodistribution of the lipid nanoparticles, as previously assessed by radiolabelling.⁴⁵ These previous experiments evidenced the integrity of the particle lipid core while circulating in blood during the first hour postinjection, with a plasma half-life of approximately 30 min, and $\approx 4\%$ radioactivity still circulating at 24 h. A similar fluorescence plasma profile is observed in the present study following LipImage™ 815 injection, supporting again the fact that the IR780-lipid dye is well anchored in the lipid core. On the contrary, very fast decay is observed for the fluorescence signal after ICG-lipidots® injection, attributed to the rapid release from the nanoparticle of the amphiphilic dye inserted at least partially in the particle shell.³³ After its release, ICG rapidly adsorbs into plasma proteins, and fluorescence decreases rapidly in the first hour following injection even if particle vectorization slightly slows down its clearance in comparison to the free dye as previously discussed.^{31,32}

Similarly to what was observed for lipidots® using radiolabelling, LipImage™ 815 distributes mainly in the liver but not in the spleen and, to a lesser extent, in adrenals and ovaries, steroid-rich organs. This tropism of the lipid nanoparticles was previously confirmed at the microscopic level by histology, evidencing moreover the specific accumulation of the particles in the parts of the organs involved in steroid hormones synthesis.⁴⁵ This original and specific distribution pattern could be accounted for by the nanometric size and lipid nature of the nanoparticles, which could confer lipoprotein-like behavior on them.

The long lasting circulation of LipImage™ 815 in blood occurs safely, and no sign of toxicity is detected during 3 weeks postinjection at the macroscopic or microscopic levels in liver, spleen, lungs, and kidneys. Such enhanced optical

properties and prolonged circulation without toxicity are very interesting for *in vivo* applications. Enhanced brightness allows more sensitive detection through deeper tissues. Long lasting particle circulation is usually associated with an augmented EPR effect that leads to a passive accumulation of nano-objects in tumor tissues.⁴⁶ We show evidence here that the stability of LipImage™ 815 allows their efficient uptake in PC3 human prostate tumors implanted in mice. Therefore, tumors are labeled during at least 3 weeks postinjection with continuous increase of the tumor-to-skin ratio during the first 10 days after injection. This prolonged fluorescence labeling of tumor tissues could allow the clear identification and time-monitoring of tumor mass margins or metastasis during surgery or during the time lapse of physical or chemical therapies to assess their efficiency in preclinical studies. The efficiency, consistency, and reliability of the EPR effect in human tumors is still an open question. However, current clinical trials using stealth and untargeted liposomes demonstrate the interest of this approach. Furthermore, the long lasting effect of LipImage™ 815 is expected to optimize the passive accumulation of these particles, even in weak EPR-positive tumors. Finally, the very long duration of the signal is also expected to avoid interindividual variations that could occur if the interval of time between injection of the contrast agent and the observation is not strictly identical. Therefore, LipImage™ 815 can be envisioned as a promising agent for *in vivo* applications requiring safe, sensitive, and long-term fluorescence imaging.

5 Conclusion

We have designed a new contrast agent, LipImage™ 815, based on lipid nanoparticle technology, now well assessed for its robustness, upscalability and biocompatibility, all features necessary for future clinical translation. LipImage™ 815 displays, as previously described ICG-lipidots®, high IC₅₀, NIR absorption and emission wavelengths in the *in vivo* “imaging window” (around 800 nm), long-term shelf colloidal and optical stabilities with high brightness ($>10^6 \text{ L mol}^{-1} \text{ cm}^{-1}$) in ready-to-use conditions (aqueous buffer). However, contrary to ICG-lipidots® for which the partial location of the dye in the particle shell induces rapid diffusion of ICG from the particles after *in vivo* injection and hence its rapid clearance, LipImage™ 815 circulates intact in blood for longer times. This new safe contrast agent can therefore accumulate by EPR effect in tumor sites, for their prolonged fluorescence labeling. This could be useful not only in the preclinical studies for everyday monitoring of the efficiencies of cancer therapies but also in the clinical field to improve the sensitivity and resolution in the detection of small cancerous nodules or tumor margins, even for in-depth tissues, through *in vivo* fluorescence imaging.

Acknowledgments

We acknowledge the Molinspiration Property Calculation Service (www.molinspiration.com) for dye logP calculation. This work is supported by the Commissariat à l’Energie Atomique et aux Energies Alternatives (CEA), by the Cancéropôle Lyon-Auvergne-Rhône-Alpes (PDC025 grant) and by a public grant overseen by the French National Research Agency (ANR) as part of the “Investissements d’Avenir” program (reference: ANR-10-NANO-01).

References

1. J. V. Frangioni, “New technologies for human cancer imaging,” *J. Clin. Oncol.* **26**(24), 4012–4021 (2008).
2. E. M. Sevick-Muraca and J. C. Rasmussen, “Molecular imaging with optics: primer and case for near-infrared fluorescence techniques in personalized medicine,” *J. Biomed. Opt.* **13**(4), 041303 (2008).
3. F. A. Jaffer and R. Weissleder, “Molecular imaging in the clinical arena,” *J. Am. Med. Assoc.* **293**(7), 855–862 (2005).
4. J. C. Rasmussen et al., “Lymphatic imaging in humans with near-infrared fluorescence,” *Curr. Opin. Biotech.* **20**(1), 74–82 (2009).
5. K. Licha and U. Resch-Genger, “Probes for optical imaging: new developments,” *Drug Discov. Today* **8**(2–4), e87–e94 (2011).
6. S. Gioux, H. S. Choi, and J. V. Frangioni, “Image-guided surgery using invisible near-infrared light: fundamentals of clinical translation,” *Mol. Imag.* **9**(5), 237–255 (2010).
7. I. Miyashiro et al., “Detection of sentinel node in gastric cancer surgery by indocyanine green fluorescence imaging: comparison with infrared imaging,” *Ann. Surg. Oncol.* **15**(6), 1640–1643 (2008).
8. Y. Ogasawara et al., “Evaluation of breast lymphatic pathways with indocyanine green fluorescence imaging in patients with breast cancer,” *World J. Surg.* **32**(9), 1924–1929 (2008).
9. E. M. Sevick-Muraca et al., “Imaging of lymph flow in breast cancer patients after microdose administration of a near-infrared fluorophore: feasibility study,” *Radiology* **246**(3), 734–741 (2008).
10. N. Tagaya et al., “Intraoperative identification of sentinel lymph nodes by near-infrared fluorescence imaging in patients with breast cancer,” *Am. J. Surg.* **195**(6), 850–853 (2008).
11. E. Tanaka et al., “Image-guided oncologic surgery using invisible light: completed pre-clinical development for sentinel lymph node mapping,” *Ann. Surg. Oncol.* **13**(12), 1671–1681 (2006).
12. S. L. Troyan et al., “The FLARE™ intraoperative near-infrared fluorescence imaging system: a first-in-human clinical trial in breast cancer sentinel lymph node mapping,” *Ann. Surg. Oncol.* **16**(10), 2943–2952 (2009).
13. E. I. Altinoglu et al., “Near-infrared emitting fluorophore-doped calcium phosphate nanoparticles for *in vivo* imaging of human breast cancer,” *ACS Nano* **2**(10), 2075–2084 (2008).
14. J. Mérian et al., “Fluorescent nanoprobes dedicated to *in vivo* imaging: from preclinical validations to clinical translation,” *Molecules* **17**(5), 5564–5591 (2012).
15. E. A. te Velde et al., “The use of fluorescent dyes and probes in surgical oncology,” *Eur. J. Surg. Oncol.* **36**(1), 6–15 (2010).
16. R. C. Benson and H. A. Kues, “Fluorescence properties of indocyanine green as related to angiography,” *Phys. Med. Biol.* **23**(1), 159–163 (1978).
17. M. L. J. Landsman et al., “Light absorbing properties, stability, and spectral stabilization of indocyanine green,” *J. Appl. Physiol.* **40**(4), 575–583 (1976).
18. E. D. Moody, P. J. Viskari, and C. L. Colyer, “Non-covalent labeling of human serum albumin with indocyanine green: a study by capillary electrophoresis with diode laser-induced fluorescence detection,” *J. Chromatogr. B Biomed. Sci. Appl.* **729**(1–2), 55–64 (1999).
19. R. Philip et al., “Absorption and fluorescence spectroscopic investigation of indocyanine green,” *J. Photochem. Photobiol. A Chem.* **96**(1–3), 137–148 (1996).
20. T. Desmettre, J. M. Devoisselle, and S. Mordon, “Fluorescence properties and metabolic features of indocyanine green (ICG) as related to angiography,” *Surv. Ophthalmol.* **45**(1), 15–27 (2000).
21. J. Choi et al., “Core-shell silica nanoparticles as fluorescent labels for nanomedicine,” *J. Biomed. Opt.* **12**(06), 064007 (2007).
22. J. M. Devoisselle et al., “A preliminary study of the *in vivo* behaviour of an emulsion formulation of Indocyanine Green,” *Laser Med. Sci.* **13**(4), 279–282 (1998).
23. R. Friedman, “Nano dot technology enters clinical trials,” *J. Natl. Cancer Inst.* **103**(19), 1428–1429 (2011).
24. M. Hutteman et al., “Randomized, double-blind comparison of indocyanine green with or without albumin premixing for near-infrared fluorescence imaging of sentinel lymph nodes in breast cancer patients,” *Breast Cancer Res. Treat.* **127**(1), 163–170 (2011).
25. T. H. Kim et al., “Filamentous, mixed micelles of triblock copolymers enhance tumor localization of indocyanine green in a murine xenograft model,” *Mol. Pharm.* **9**(1), 135–143 (2012).

26. N. Larson and H. Ghandehari, "Polymeric conjugates for drug delivery," *Chem. Mater.* **24**(5), 840–853 (2012).
27. E. Portnoy et al., "Cetuximab-labeled liposomes containing near-infrared probe for in vivo imaging," *Nanomedicine Nanotech. Biol. Med.* **7**(4), 480–488 (2011).
28. V. Saxena, M. Sadoqi, and J. Shao, "Enhanced photo-stability, thermal-stability and aqueous-stability of indocyanine green in polymeric nanoparticulate systems," *J. Photochem. Photobiol. B Biol.* **74**(1), 29–38 (2004).
29. M. A. Yaseen et al., "Biodistribution of encapsulated indocyanine green in healthy mice," *Mol. Pharm.* **6**(5), 1321–1332 (2009).
30. M. A. Yaseen et al., "In-vivo fluorescence imaging of mammalian organs using charge-assembled mesocapsule constructs containing indocyanine green," *Opt. Express* **16**(25), 20577–20587 (2008).
31. F. P. Navarro et al., "Lipid nanoparticle vectorization of IndoCyanine Green improves fluorescence imaging for tumor diagnosis and lymph node resection," *J. Biomed. Nanotechnol.* **8**(5), 730–741 (2012).
32. F. P. Navarro et al., "Cell tolerability and biodistribution in mice of indocyanine green-loaded lipid nanoparticles," *J. Biomed. Nanotechnol.* **8**(4), 594–604 (2012).
33. J. Mérian et al., "Impact of dyes structural properties on their localization in lipid nanoparticles and their in vivo release mechanism," in preparation.
34. J. Gravier et al., "Lipidots: competitive organic alternative to quantum dots for in vivo fluorescence imaging," *J. Biomed. Opt.* **16**(9), 096013 (2011).
35. J. V. Frangioni, "In vivo near-infrared fluorescence imaging," *Curr. Opin. Chem. Biol.* **7**(5), 626–634 (2003).
36. R. Weissleder and V. Ntziachristos, "Shedding light onto live molecular targets," *Nat. Med.* **9**(1), 123–128 (2003).
37. T. Delmas et al., "Preparation and characterization of highly stable lipid nanoparticles with amorphous core of tuneable viscosity," *J. Colloid Interf. Sci.* **360**(2), 471–481 (2011).
38. T. Delmas et al., "How to prepare and stabilize very small nanoemulsions," *Langmuir* **27**(5), 1683–1692 (2011).
39. D. Oushiki et al., "Development and application of a near-infrared fluorescence probe for oxidative stress based on differential reactivity of linked cyanine dyes," *J. Am. Chem. Soc.* **132**(8), 2795–2801 (2010).
40. R. C. Benson and H. A. Kues, "Absorption and fluorescence properties of cyanine dyes," *J. Chem. Eng. Data* **22**(4), 379–383 (1977).
41. S. Gioux et al., "FluoSTIC: miniaturized fluorescence image-guided surgery system," *J. Biomed. Opt.* **17**(10), 109802 (2012).
42. W. Pham et al., "A near-infrared dye for multichannel imaging," *Chem. Commun.* 1895–1897 (2008).
43. M. Goutayer et al., "Tumor targeting of functionalized lipid nanoparticles: assessment by in vivo fluorescence imaging," *Eur. J. Pharm. Biopharm.* **75**(2), 137–147 (2010).
44. I. Texier et al., "Cyanine-loaded lipid nanoparticles for improved in vivo fluorescence imaging," *J. Biomed. Opt.* **14**(5), 054005 (2009).
45. J. Mérian et al., "Synthetic lipid nanoparticles targeting steroid organs," *J. Nucl. Med.*, accepted for publication.
46. J. Fang, H. Nakamura, and H. Maeda, "The EPR effect: unique features of tumor blood vessels for drug delivery, factors involved, and limitations and augmentation of the effect," *Adv. Drug Deliv. Rev.* **63**(3), 136–151 (2011).